

# Boundary-layer control with unstructured uncertainties with application to adaptive autopilots

Peng Li, Di Liu *Member, IEEE*, and Simone Baldi *Senior member, IEEE*

**Abstract**—Control with unstructured uncertainties refers to controlling systems where not only the parameters are unknown, but also the way the parameters appear in the dynamics. This problem is of particular significance in autopilots, where a unified control architecture for vehicles with different structures (aerial/ground/marine) is sought. By only making use of basic Euler-Lagrange properties valid in most mechanical systems independently of their specific structure, this brief proposes an adaptive design that does not rely on structural knowledge of the uncertainties. The proposed adaptive method, here validated in the ArduPlane module of ArduPilot, applies also to other modules like ArduCopter, ArduRover, ArduSub. Enhanced performance with respect to state-of-the-art methods addressing unstructured and state-dependent uncertainties is verified.

**Note:** *This document is to be intended as a technical report with more comparative tests than a brief paper currently under review.*

**Index Terms**—Unstructured uncertainty, state-dependent uncertainty, unmanned vehicles, autopilot, adaptive control

## I. INTRODUCTION

Autopilots are key control components of unmanned aerial [1]–[3], ground [4], [5], and marine vehicles [6]. A challenging task for autopilots is to handle large uncertainty stemming from parametric perturbations, unmodeled dynamics [7], [8], measurement noises and environmental disturbances [9], [10]. It is known that mismatches between a priori assumptions on the uncertainty and reality may fool the control law, degrade performance, and even lose stability [11]. This issue is particularly significant in autopilots: as most autopilot suites aim at unified control architectures to tackle aerial/ground/marine vehicles with different structures (cf. the ArduPlane, ArduCopter, ArduRover, ArduSub modules in ArduPilot, or similar modules in other autopilots), avoiding structural assumptions on system dynamics and uncertainty plays a key role in this field.

As unmanned vehicles are mechanical systems, a convenient research perspective to autopilot design comes from the control of uncertain Euler-Lagrange dynamics. These control methods can be roughly categorized according to robust methods and adaptive methods. Common robust methods, based on observers [12], passivity [13], or sliding mode control (SMC) [14], [15], eventually rely on some prior knowledge of the uncertainty, making it difficult to cope with uncertainties going beyond the expected bounds during system operation [11]. Even adaptive methods are not free of prior knowledge of the uncertainty, appearing in the form of structural conditions

P. Li is with School of Cyber Science and Engineering, Southeast University, Nanjing, China (email: 1peng\_2013@163.com)

D. Liu is with School of Computation, Information and Technology, Technische Universität München (TUM), Germany (email: di.liu@tum.de)

S. Baldi is with Frontier Center for Mobile Information Communication and Security, Southeast University, China, and with Delft Center for Systems and Control, TU Delft, The Netherlands (email: s.baldi@tudelft.nl)

(e.g. linear-in-parameter, matching conditions [16], [17]), or of assumptions on uncertainty and its time derivative being upper bounded by possibly unknown constants [18]–[21].

Recent years have seen progress in the control of Euler-Lagrange dynamics with reduced structural knowledge [22]–[25], motivated by the observation that most uncertainty is state-dependent, so that imposing constant upper bounds restrictively amount to assuming a priori bounded states before proving stability [26]. Despite the progress, achieving finite-time stability in spite of unstructured uncertainties remains an open issue: available methods for finite-time convergence also rely on structural conditions on the uncertainty [27]–[30]. Embedding control designs with reduced structural knowledge into unified autopilot architectures is another notable open issue. The main contribution of this work are:

- Proposing a novel sliding surface that embeds a non-singular finite-time term and an integral term, useful to incorporate control law into existing autopilot loops.
- Removing structural knowledge of the uncertainty. Only basic Euler-Lagrange properties are used, valid for mechanical systems independently on their specific structure.
- Proposing an adaptive law in the framework of finite-time control to tackle unstructured uncertainty. The adaptive law is designed to estimate a state-dependent upper bound of the uncertainty, whose form is independent on the specific structure of the system.

The paper is organized as follows: Section II formulates the problem of control with unstructured uncertainty. Section III covers the design of the adaptive control law and its stability analysis. Software-in-the-loop validations are in Section IV, where the proposed approach is compared to a standard PID autopilot (e.g. the existing ArduPlane module of ArduPilot), to a robust SMC autopilot, and to an adaptive SMC autopilot stemming from previous work by the authors. Conclusions are in Section V.

**Notations:** Let  $\mathbb{R}$  and  $\mathbb{R}^{n \times m}$  be the sets of real numbers and real  $n \times m$  matrices, and  $\mathbb{I}_n$  be the  $n \times n$  identity matrix. Vectors are denoted with bold, such as  $\mathbf{x} = [x_1, \dots, x_n]^T$ . Let us use the short notations  $\text{sign}(\mathbf{x}) = [\text{sign}(x_1), \dots, \text{sign}(x_n)]^T$ ,  $\text{sig}^v(\mathbf{x}) = [|x_1|^v \text{sign}(x_1), \dots, |x_n|^v \text{sign}(x_n)]^T$ . Let  $\|\cdot\|$  and  $\lambda_{\min}(\cdot)$  denote the Euclidean norm and minimum eigenvalue.

## II. PRELIMINARIES AND PROBLEM FORMULATION

Consider the following Euler-Lagrange (EL) dynamics

$$\mathbf{M}(\mathbf{q})\ddot{\mathbf{q}} + \mathbf{C}(\mathbf{q}, \dot{\mathbf{q}})\dot{\mathbf{q}} + \mathbf{G}(\mathbf{q}) + \mathbf{F}(\dot{\mathbf{q}}) + \mathbf{d} = \mathbf{u}, \quad (1)$$

with  $\mathbf{q}, \dot{\mathbf{q}}, \ddot{\mathbf{q}} \in \mathbb{R}^n$  denoting the state and its time derivatives,  $\mathbf{M}(\mathbf{q}) \in \mathbb{R}^{n \times n}$  the mass/inertia matrix,  $\mathbf{C}(\mathbf{q}, \dot{\mathbf{q}}) \in \mathbb{R}^{n \times n}$  the

Coriolis matrix,  $\mathbf{G}(\mathbf{q}) \in \mathbb{R}^n$  the gravity term,  $\mathbf{F}(\dot{\mathbf{q}}) \in \mathbb{R}^n$  the damping/friction term,  $\mathbf{d} \in \mathbb{R}^n$  the external disturbance, and  $\mathbf{u} \in \mathbb{R}^n$  the control input.

The Euler-Lagrange dynamics (1) can describe several real-world mechanical systems, such as robotic manipulators and aerial/ground/marine vehicles [22], [23], [26]. For all such systems, the following standard properties hold:

**Property 1:** There exist  $c, g, f, d \in \mathbb{R}^+$  such that  $\|\mathbf{C}(\mathbf{q}, \dot{\mathbf{q}})\| \leq c\|\dot{\mathbf{q}}\|$ ,  $\|\mathbf{G}(\mathbf{q})\| \leq g$ ,  $\|\mathbf{F}(\dot{\mathbf{q}})\| \leq f\|\dot{\mathbf{q}}\|$  and  $\|\mathbf{d}(t)\| \leq d$ .

**Property 2:** The matrix  $\mathbf{M}(\mathbf{q})$  is symmetric and uniformly positive, that is,  $\exists m_1, m_2 \in \mathbb{R}^+$  such that

$$0 < m_1 \mathbb{I}_n \leq \mathbf{M}(\mathbf{q}) \leq m_2 \mathbb{I}_n. \quad (2)$$

**Property 3:** The matrix  $\dot{\mathbf{M}}(\mathbf{q}) - 2\mathbf{C}(\mathbf{q}, \dot{\mathbf{q}})$  is skew symmetric i.e.  $\mathbf{x}^T(\dot{\mathbf{M}}(\mathbf{q}) - 2\mathbf{C}(\mathbf{q}, \dot{\mathbf{q}}))\mathbf{x} = 0$  for any non-zero vector  $\mathbf{x}$ .

**Remark 1** (Unstructured uncertainty). *Properties 1-3 do not rely on the specific structure of the system. The structure of  $\mathbf{M}, \mathbf{C}, \mathbf{F}, \mathbf{G}, \mathbf{d}$  in (1) and the knowledge of  $m_1, m_2, c, g, f, d$  in their corresponding bounds will be unknown in this work.*

Let us recall and extend a Lyapunov characterization of practical finite-time stability, to be used for stability analysis:

**Lemma 1** [31]: *Consider general nonlinear dynamics*

$$\dot{x} = g(t, x), \quad x(0) = x_0, \quad (3)$$

with  $g : \mathbb{R}_+ \times \mathbb{R}^n \mapsto \mathbb{R}^n$  a continuous function satisfying  $g(t, 0) = 0, \forall t$ . Suppose there exists a positive definite and continuous radially unbounded function  $V(x) : \mathbb{R}^n \mapsto \mathbb{R}$  such that  $\dot{V}(x) \leq -\eta V^{\frac{1+v}{2}}(x) + \omega$ , where  $\eta > 0$ ,  $0 < v \leq 1$ ,  $\omega < \infty$ . Then, the origin of (3) is practical finite-time stable and the state  $x$  converges in finite time to the region

$$\Psi = \{x \mid V^{\frac{1+v}{2}}(x) \leq \frac{\omega}{(1-\nu)\eta}\}, \quad 0 < \nu < 1$$

where an estimate for the finite time  $T_s$  is

$$T_s = \frac{2}{(1-v)\nu\eta} \left[ V^{\frac{1-v}{2}}(x(0)) - \left( \frac{\omega}{(1-\nu)\eta} \right)^{\frac{1-v}{1+v}} \right], \quad \text{if } 0 < v < 1,$$

and, by using L'Hôpital's rule for  $\lim_{v \rightarrow 1} T_s$ ,

$$T_s = \frac{1}{\nu\eta} [\ln V(x(0))\omega - \ln(1-\nu)\eta], \quad \text{if } v = 1.$$

Denote with  $\mathbf{q}_d, \dot{\mathbf{q}}_d, \ddot{\mathbf{q}}_d \in \mathbb{R}^n$  the desired state and its derivatives, which satisfy  $\|\dot{\mathbf{q}}_d(t)\| \leq q_m$ ,  $\|\ddot{\mathbf{q}}_d(t)\| \leq q_{mm}$ ,  $\forall t$ . The following control question arises:

**Problem:** Without structural knowledge of the terms in (1) and of their bounds as in Remark 1, find a control  $\mathbf{u}(\cdot)$  such that the origin of the EL closed loop is practical finite-time stable with finite-time convergence of the tracking error  $\mathbf{e} = \mathbf{q} - \mathbf{q}_d$ .

### III. SLIDING SURFACE AND ADAPTIVE CONTROL DESIGN

The design is organized as follows: first, a novel sliding surface is proposed; then, the uncertainties affecting the error dynamics are analyzed (Sect. III-A), leading to an adaptive law to compensate them (Sect. III-B). The proposed sliding surface is

$$\mathbf{s} = \dot{\mathbf{e}} + \lambda_1 \mathbf{e} + \lambda_2 \int_0^t \mathbf{e}(\tau) d\tau + \lambda_3 \Delta(\mathbf{e}), \quad (4)$$

where  $\lambda_k, k = 1, 2, 3$  are positive definite diagonal matrices with entries  $\lambda_{ki}$ ,  $i = 1, 2, \dots, n$ , and  $\Delta(\mathbf{e})$  is a vector with entries  $\Delta_i(e_i)$  defined as

$$\Delta_i(e_i) = \begin{cases} \text{sig}^\gamma(e_i), & \text{if } |e_i| > \varepsilon, \\ \alpha_1 e_i + \alpha_2 \text{sign}(e_i) e_i^2, & \text{if } |e_i| \leq \varepsilon. \end{cases} \quad (5)$$

where  $0 < \gamma < 1$ ,  $\varepsilon$  is a small positive constant, and

$$\alpha_1 = (2 - \gamma)\varepsilon^{\gamma-1}, \quad \alpha_2 = (\gamma - 1)\varepsilon^{\gamma-2}.$$

The time derivative of  $\mathbf{s}$  is well defined in the entire state space

$$\dot{\mathbf{s}} = \ddot{\mathbf{e}} + \lambda_1 \dot{\mathbf{e}} + \lambda_2 \mathbf{e} + \lambda_3 \dot{\Delta}(\mathbf{e}), \quad (6)$$

with the entries of  $\dot{\Delta}(\mathbf{e})$  being

$$\dot{\Delta}_i(e_i) = \begin{cases} \gamma |e_i|^{\gamma-1} \dot{e}_i, & \text{if } |e_i| > \varepsilon \\ (\alpha_1 + 2\alpha_2 |e_i|) \dot{e}_i, & \text{if } |e_i| \leq \varepsilon. \end{cases} \quad (7)$$

Note that the parameters  $\alpha_1, \alpha_2$  ensure continuity of  $\mathbf{s}$  and  $\dot{\mathbf{s}}$  at the point  $|e_i| = \varepsilon$ . The following lemma provides appropriate bounds on  $\Delta(\mathbf{e})$  and  $\dot{\Delta}(\mathbf{e})$ , useful for stability analysis:

**Lemma 2:** *For  $\Delta(\mathbf{e}), \dot{\Delta}(\mathbf{e})$  in (5) and (7), the following holds*

$$\|\Delta(\mathbf{e})\| \leq \|\text{sig}^\gamma(\mathbf{e})\|, \quad \|\dot{\Delta}(\mathbf{e})\| \leq \alpha_1 \|\dot{\mathbf{e}}\|. \quad (8)$$

*Proof.* To prove the first bound in (8), substitute  $\alpha_1, \alpha_2$  into (5) and define the function  $f(|e_i|, \varepsilon) = (2 - \gamma)\varepsilon^{\gamma-1}|e_i| + (\gamma - 1)\varepsilon^{\gamma-2}|e_i|^2$ ,  $\varepsilon \geq |e_i|$ . We have

$$\frac{\partial f(|e_i|, \varepsilon)}{\partial \varepsilon} = (\gamma - 1)(\gamma - 2)|e_i|\varepsilon^{\gamma-3}(|e_i| - \varepsilon),$$

which implies that the gradient of  $f(|e_i|, \varepsilon)$  with respect to  $\varepsilon$  is negative if  $\varepsilon \geq |e_i|$ . So  $f(|e_i|, \varepsilon)$  is monotonically decreasing with respect to  $\varepsilon$ , which implies

$$f(|e_i|, \varepsilon) \leq f(|e_i|, |e_i|) = |e_i|^\gamma. \quad (9)$$

Substituting (9) into (5) gives  $|\Delta_i(e_i)| \leq |e_i|^\gamma$ , from which we conclude that  $\|\Delta(\mathbf{e})\| \leq \|\text{sig}^\gamma(\mathbf{e})\|$ .

To prove the second bound in (8), define the function

$$g(|e_i|) = \begin{cases} \gamma |e_i|^{\gamma-1}, & \text{if } |e_i| > \varepsilon, \\ \alpha_1 + 2\alpha_2 |e_i|, & \text{if } |e_i| \leq \varepsilon. \end{cases}$$

The function  $g(|e_i|)$  is monotonically decreasing with respect to  $|e_i|$  because of  $0 < \gamma < 1$  and  $\alpha_2 < 0$ , which implies

$$g(|e_i|) \leq g(0) = \alpha_1. \quad (10)$$

Substituting (10) into (7) gives  $|\dot{\Delta}_i(e_i)| \leq \alpha_1 |\dot{e}_i|$ , from which we conclude that  $\|\dot{\Delta}(\mathbf{e})\| \leq \alpha_1 \|\dot{\mathbf{e}}\|$ .  $\square$

#### A. Uncertainty structure

Based on the proposed sliding surface (4), a suitable upper bound structure for the uncertainty of (1) will be derived. Multiplying (6) by  $\mathbf{M}$  and using (1) we obtain

$$\begin{aligned} \mathbf{M}\dot{\mathbf{s}} &= \mathbf{M}\lambda_1 \dot{\mathbf{e}} + \mathbf{M}\lambda_2 \mathbf{e} + \mathbf{M}\lambda_3 \dot{\Delta}(\mathbf{e}) + \mathbf{M}(\ddot{\mathbf{q}} - \ddot{\mathbf{q}}_d) \\ &= \mathbf{u} - \mathbf{Cs} + \varphi, \end{aligned} \quad (11)$$

where

$$\begin{aligned} \varphi &\triangleq -(\mathbf{C}\dot{\mathbf{q}} + \mathbf{G} + \mathbf{F} + \mathbf{d}) \\ &\quad + \mathbf{M}\ddot{\mathbf{q}}_d - \mathbf{M}\lambda_1 \dot{\mathbf{e}} - \mathbf{M}\lambda_2 \mathbf{e} - \mathbf{M}\lambda_3 \dot{\Delta}(\mathbf{e}) - \mathbf{Cs}, \end{aligned} \quad (12)$$

represents an aggregate state-dependent uncertainty. By combining (4) and Properties 1-2, we obtain the following (state-dependent) bound for such uncertainty

$$\begin{aligned} \|\varphi\| &\leq c\|\dot{\mathbf{q}}\|^2 + g + f\|\dot{\mathbf{q}}\| + d \\ &+ m_2(\|\ddot{\mathbf{q}}_d\| + \|\boldsymbol{\lambda}_1\|\|\dot{\mathbf{e}}\| + \|\boldsymbol{\lambda}_2\|\|\mathbf{e}\| + \|\boldsymbol{\lambda}_3\|\|\dot{\Delta}(\mathbf{e})\|) \\ &+ c\|\dot{\mathbf{q}}\|(\|\dot{\mathbf{e}}\| + \|\boldsymbol{\lambda}_1\|\|\mathbf{e}\| + \|\boldsymbol{\lambda}_2\|\|\int_0^t \mathbf{e}(\tau)d\tau\| \\ &+ \|\boldsymbol{\lambda}_3\|\|\Delta(\mathbf{e})\|). \end{aligned} \quad (13)$$

Define

$$\boldsymbol{\xi}(t) = \left[ (\mathbf{e} + \text{sig}^\gamma(\mathbf{e}))^T(t) \quad \dot{\mathbf{e}}^T(t) \quad (\int_0^t \mathbf{e}(\tau)d\tau)^T \right]^T.$$

Clearly, the following inequalities hold

$$\begin{aligned} \|\boldsymbol{\xi}(t)\| &\geq \|\mathbf{e}(t)\|, \quad \|\boldsymbol{\xi}(t)\| \geq \|\text{sig}^\gamma(\mathbf{e})(t)\|, \\ \|\boldsymbol{\xi}(t)\| &\geq \|\dot{\mathbf{e}}(t)\|, \quad \|\boldsymbol{\xi}(t)\| \geq \|\int_0^t \mathbf{e}(\tau)d\tau\|. \end{aligned} \quad (14)$$

According to Lemma 2 and (14), we have

$$\|\varphi\| \leq \theta_0^* + \theta_1^*\|\boldsymbol{\xi}(t)\| + \theta_2^*\|\boldsymbol{\xi}(t)\|^2, \quad (15)$$

where  $\theta_0^*$ ,  $\theta_1^*$ ,  $\theta_2^*$  are positive constants defined as

$$\theta_0^* \triangleq cq_m^2 + g + fq_m + d + m_2q_{mm},$$

$$\theta_1^* \triangleq cq_m(3 + \|\boldsymbol{\lambda}_1\| + \|\boldsymbol{\lambda}_2\| + \|\boldsymbol{\lambda}_3\|) + f + m_2(\|\boldsymbol{\lambda}_1\| + \|\boldsymbol{\lambda}_2\| + \|\boldsymbol{\lambda}_3\|\alpha_1),$$

$$\theta_2^* \triangleq c(2 + \|\boldsymbol{\lambda}_1\| + \|\boldsymbol{\lambda}_2\| + \|\boldsymbol{\lambda}_3\|).$$

Note that these constants are unknown in line with Remark 1.

### B. Adaptive control law

Aiming at compensating the uncertainty (15), the following control input is proposed

$$\mathbf{u}(t) = -\boldsymbol{\Lambda}\mathbf{s}(t) - \rho(t)\text{sign}(\mathbf{s}(t)) - \sigma\text{sig}^v(\mathbf{s}(t)), \quad (16)$$

with  $\boldsymbol{\Lambda}$  a positive definite matrix,  $\mu > 0$ ,  $\sigma > 0$ ,  $0 < v \leq 1$ , and

$$\rho(t) = \hat{\theta}_0(t) + \hat{\theta}_1(t)\|\boldsymbol{\xi}(t)\| + \hat{\theta}_2(t)\|\boldsymbol{\xi}(t)\|^2. \quad (17)$$

The gains  $\hat{\theta}_i$ ,  $i = 0, 1, 2$  can be interpreted as estimates of  $\theta_i^*$  in (15), updated by the following adaptive laws

$$\dot{\hat{\theta}}_i(t) = \|\mathbf{s}(t)\|\|\boldsymbol{\xi}(t)\|^i - \beta_i\hat{\theta}_i^v(t), \quad \hat{\theta}_i(0) > 0 \quad (18)$$

where  $\beta_i$ ,  $i = 0, 1, 2$  are positive constants. We now analyze the stability properties of the proposed method.

**Lemma 3:** Consider the adaptive laws in (18) with initial condition  $\hat{\theta}_i(0) > 0$ . Then,  $\hat{\theta}_i(t) \geq 0$ ,  $\forall t \geq 0$ .

*Proof.* We use a proof by contradiction. Assume that  $\exists \hat{\theta}_i(t) < 0$  under initial condition  $\hat{\theta}_i(0) > 0$ . Then, there must exist  $0 < \tau < t$  such that  $\hat{\theta}_i(\tau) = 0$  and  $\dot{\hat{\theta}}_i(\tau) < 0$  because of continuity of  $\hat{\theta}_i(t)$ . However, substituting  $\hat{\theta}_i(\tau) = 0$  into (18) gives  $\dot{\hat{\theta}}_i(\tau) = \|\mathbf{s}(\tau)\|\|\boldsymbol{\xi}(\tau)\|^i \geq 0$ , which does not satisfy the previously assumed negative time derivative. This verifies that  $\hat{\theta}_i(t) \geq 0$ ,  $\forall t \geq 0$  hold under initial condition  $\hat{\theta}_i(0) > 0$ .  $\square$

**Theorem 1.** Under Properties 1-3, the origin of the closed-loop Euler-Lagrange dynamics (1) with control law (16)-(17) and adaptive law (18), are practical finite-time stable. Let  $\bar{s}$

be the bound for  $\mathbf{s}$  in (4) after finite time: then, the tracking error  $\mathbf{e}$  converges in finite time to the region

$$\Phi = \max\{\varepsilon, \frac{\bar{s}}{\min_i\{\lambda_{1i}\}}, \left(\frac{\bar{s}}{\min_i\{\lambda_{3i}\}}\right)^{\frac{1}{\gamma}}\}.$$

*Proof.* Select the Lyapunov function candidate:

$$V(\mathbf{s}, \tilde{\theta}) = \frac{1}{2}\mathbf{s}^T \mathbf{M} \mathbf{s} + \frac{1}{2} \sum_{i=0}^2 \tilde{\theta}_i^2 \quad (19)$$

with  $\tilde{\theta}_i = \theta_i^* - \hat{\theta}_i$ . The time derivative of  $V$  along the dynamics (11), (16) is

$$\begin{aligned} \dot{V} &= \mathbf{s}^T(\mathbf{u} - \mathbf{Cs} + \boldsymbol{\varphi}) + \frac{1}{2}\mathbf{s}^T \dot{\mathbf{M}} \mathbf{s} - \sum_{i=0}^2 \tilde{\theta}_i \dot{\hat{\theta}}_i \\ &= \mathbf{s}^T(-\boldsymbol{\Lambda}\mathbf{s} - \rho\text{sign}(\mathbf{s}) - \sigma\text{sig}^v(\mathbf{s}) + \boldsymbol{\varphi}) + \frac{1}{2}\mathbf{s}^T(\dot{\mathbf{M}} - 2\mathbf{C})\mathbf{s} - \sum_{i=0}^2 \tilde{\theta}_i \dot{\hat{\theta}}_i. \end{aligned}$$

Using Property 3, we obtain

$$\dot{V} = -\mathbf{s}^T \boldsymbol{\Lambda} \mathbf{s} - \sigma \mathbf{s}^T \text{sig}^v(\mathbf{s}) + \mathbf{s}^T \boldsymbol{\varphi} - \rho \mathbf{s}^T \text{sign}(\mathbf{s}) - \sum_{i=0}^2 \tilde{\theta}_i \dot{\hat{\theta}}_i.$$

Since  $\rho > 0$  from Lemma 3, substituting (15), (17) and (18) in the Lyapunov time derivative gives

$$\begin{aligned} \dot{V} &\leq -\mathbf{s}^T \boldsymbol{\Lambda} \mathbf{s} - \sigma \mathbf{s}^T \text{sig}^v(\mathbf{s}) + \sum_{i=0}^2 \tilde{\theta}_i (\|\boldsymbol{\xi}\|^i \|\mathbf{s}\| - \dot{\hat{\theta}}_i) \\ &\leq -\mathbf{s}^T \boldsymbol{\Lambda} \mathbf{s} - \sigma \sum_{i=1}^n (|s_i|^2)^{\frac{1+v}{2}} + \sum_{i=0}^2 \beta_i \tilde{\theta}_i \dot{\hat{\theta}}_i^v. \end{aligned} \quad (20)$$

In line with Lemma 1, we cover the cases  $0 < v < 1$  and  $v = 1$ , to make the design more flexible.

*Design (a):*  $0 < v < 1$ . Using Lemma 3 and the definitions of  $\theta_i^*$ ,  $\tilde{\theta}_i$ , we have  $\theta_i^* > 0$ ,  $\dot{\hat{\theta}}_i \geq 0$ , and  $\tilde{\theta}_i \leq \theta_i^*$ . Then, let us analyze the term  $\tilde{\theta}_i \dot{\hat{\theta}}_i^v$  by making use of [32, Lemmas 4,5]

$$\begin{aligned} \tilde{\theta}_i \dot{\hat{\theta}}_i^v &= \hat{\theta}_i^v(\theta_i^* - \hat{\theta}_i) \\ &\leq \frac{1}{1+v}(\theta_i^{*1+v} - \hat{\theta}_i^{1+v}) \leq \frac{1}{1+v}(\theta_i^{*1+v} - (\theta_i^* - |\tilde{\theta}_i|)^{1+v}) \\ &\leq \frac{1}{1+v}(\theta_i^{*1+v} - (|\tilde{\theta}_i|^{1+v} - \theta_i^{*1+v})) = \frac{1}{1+v}(2\theta_i^{*1+v} - |\tilde{\theta}_i|^{1+v}). \end{aligned} \quad (21)$$

Substituting (21) into (20) gives

$$\begin{aligned} \dot{V} &\leq -\lambda_{\min}(\boldsymbol{\Lambda})\|\mathbf{s}\|^2 - \sigma \sum_{i=1}^n (|s_i|^2)^{\frac{1+v}{2}} \\ &\quad - \frac{1}{1+v} \sum_{i=0}^2 \beta_i |\tilde{\theta}_i|^{1+v} + \frac{2}{1+v} \sum_{i=0}^2 \beta_i \theta_i^{*1+v} \\ &\leq -\sigma \sum_{i=1}^n (|s_i|^2)^{\frac{1+v}{2}} - \frac{1}{1+v} \sum_{i=0}^2 \beta_i (|\tilde{\theta}_i|^2)^{\frac{1+v}{2}} + \frac{2}{1+v} \sum_{i=0}^2 \beta_i \theta_i^{*1+v}. \end{aligned}$$

Then, using [33, Lemma 1] we have

$$\dot{V} \leq -\eta_1 \left( \frac{m_2}{2} \sum_{i=1}^n |s_i|^2 + \frac{1}{2} \sum_{i=0}^2 |\tilde{\theta}_i|^2 \right)^{\frac{1+v}{2}} + \omega_1, \quad (22)$$

where  $\eta_1 = \min_i \left\{ \frac{2\sigma}{m_2}, \frac{2\beta_i}{1+v} \right\} > 0$  and  $\omega_1 = \frac{2}{1+v} \sum_{i=0}^2 \beta_i \theta_i^{*1+v} > 0$ . The Lyapunov function (19) can be upper bounded as

$$V \leq \frac{m_2}{2} \|\mathbf{s}\|^2 + \frac{1}{2} \sum_{i=0}^2 |\tilde{\theta}_i|^2, \quad (23)$$

and substituting (23) into (22) gives

$$\dot{V} \leq -\eta_1 V^{\frac{1+v}{2}} + \omega_1. \quad (24)$$

We conclude from Lemma 1 that the states  $(\mathbf{s}, \tilde{\theta})$  are driven to the region  $\Psi$  in finite-time  $T_s$ , where

$$\begin{aligned} \Psi &= \{\mathbf{s}, \tilde{\theta} \mid V^{\frac{1+v}{2}}(\mathbf{s}, \tilde{\theta}) \leq \frac{\omega_1}{(1-\iota)\eta_1}\}, \quad 0 < \iota < 1, \\ T_s &= \frac{2}{(1-v)\iota\eta_1} \left[ V^{\frac{1-v}{2}}(\mathbf{s}(0), \tilde{\theta}(0)) - \left( \frac{\omega_1}{(1-\iota)\eta_1} \right)^{\frac{1-v}{1+v}} \right]. \end{aligned}$$

*Design (b):*  $v = 1$ . Note that (20) reduces to

$$\dot{V} \leq -\mathbf{s}^T \mathbf{\Lambda} \mathbf{s} + \sum_{i=0}^2 \beta_i \tilde{\theta}_i \hat{\theta}_i.$$

With analogous steps as design (a), we have that the states  $(\mathbf{s}, \tilde{\theta})$  are driven to the region  $\Psi$  in finite-time  $T_s$ , where

$$\begin{aligned} \Psi &= \{\mathbf{s}, \tilde{\theta} \mid V^{\frac{1+v}{2}}(\mathbf{s}, \tilde{\theta}) \leq \frac{\omega_2}{(1-\iota)\eta_2}\}, \\ T_s &= \frac{1}{\iota\eta_2} [\ln V(\mathbf{s}(0), \tilde{\theta}(0)) \omega_2 - \ln(1-\iota)\eta_2], \end{aligned}$$

where  $\eta_2 = \frac{\min_i \{\lambda_{\min}(\mathbf{\Lambda}), \beta_i/2\}}{\max_i \{m_2/2, 1/2\}} > 0$  and  $\omega_2 = \frac{1}{2} \sum_{i=0}^2 \beta_i \theta_i^{*2} > 0$ .

To find a bound for the tracking error, consider the Lyapunov function  $V_e = \frac{1}{2} e_i^2 + \frac{1}{2} \lambda_{2i} (\int_0^t e_i(\tau) d\tau)^2$ , giving

$$\dot{V}_e = e_i \dot{e}_i + \lambda_{2i} e_i \int_0^t e_i(\tau) d\tau. \quad (25)$$

Then, we proceed along two cases as follows.

*Case I:*  $|e_i| > \varepsilon$ . According to (4) and (5) we have

$$\dot{e}_i + \lambda_{1i} e_i + \lambda_{2i} \int_0^t e_i(\tau) d\tau + \lambda_{3i} \text{sig}^\gamma(e_i) = s_i, \quad (26)$$

which can be rewritten in three different forms as

$$\dot{e}_i + \left( \lambda_{1i} - \frac{s_i}{e_i} \right) e_i + \lambda_{2i} \int_0^t e_i(\tau) d\tau + \lambda_{3i} \text{sig}^\gamma(e_i) = 0, \quad (27)$$

$$\dot{e}_i + \lambda_{1i} e_i + \left( \lambda_{2i} - \frac{s_i}{\int_0^t e_i(\tau) d\tau} \right) \int_0^t e_i(\tau) d\tau + \lambda_{3i} \text{sig}^\gamma(e_i) = 0, \quad (28)$$

$$\dot{e}_i + \lambda_{1i} e_i + \lambda_{2i} \int_0^t e_i(\tau) d\tau + \left( \lambda_{3i} - \frac{s_i}{\text{sig}^\gamma(e_i)} \right) \text{sig}^\gamma(e_i) = 0. \quad (29)$$

Note that substituting the condition  $s_i = 0$  into (4) gives

$$\dot{e}_i = -(\lambda_{1i} e_i + \lambda_{2i} \int_0^t e_i(\tau) d\tau + \lambda_{3i} \Delta_i(e_i)). \quad (30)$$

Then, substituting (30) into (25) gives

$$\dot{V}_e = -e_i (\lambda_{1i} e_i + \lambda_{3i} \Delta_i(e_i)) = -\lambda_{1i} e_i^2 - \lambda_{3i} |e_i|^{\gamma+1} \leq 0.$$

In the following, let us analyze the tracking errors assuming (30) holds. The fact that  $V_e > 0$  and  $\dot{V}_e \leq 0$  implies  $\lim_{t \rightarrow \infty} V_e(t) = V_e(\infty) < V_e(0)$ , that is,  $e_i$  and  $\int_0^t e_i(\tau) d\tau$

are bounded. Meanwhile,  $\dot{e}_i$  is also bounded according to (30). Furthermore, by integrating  $\dot{V}_e$ , we have

$$\lim_{t \rightarrow \infty} \int_0^t \lambda_{1i} e_i^2(\tau) + \lambda_{3i} |e_i|^{\gamma+1}(\tau) d\tau = V_e(0) - V_e(\infty),$$

which implies that  $e_i$  has bounded 2-norm. Thus, assuming (30) holds, we get  $e_i \rightarrow 0$  from Barbalat's lemma. An ultimate bound for  $\int_0^t e_i(\tau) d\tau$  is obtained noting that, for zero initial conditions of the integrator,  $V_e(\infty) < V_e(0) = \frac{1}{2} e_i^2(0)$ , and  $V_e(\infty) = \frac{1}{2} e_i^2(\infty) + \lim_{t \rightarrow \infty} \frac{1}{2} \lambda_{2i} (\int_0^t e_i^2(\tau) d\tau)^2 < \frac{1}{2} e_i^2(0)$ . This gives  $\frac{|e_i(0)|}{\sqrt{\lambda_{2i}}}$  as an ultimate bound for  $|\int_0^t e_i(\tau) d\tau|$ .

With this in mind, we notice that (27), (28) and (29) are in the form of (30) whenever

$$\lambda_{1i} - \frac{s_i}{e_i} > 0, \quad \lambda_{2i} - \frac{s_i}{\int_0^t e_i(\tau) d\tau} > 0, \quad \lambda_{3i} - \frac{s_i}{\text{sig}^\gamma(e_i)} > 0.$$

This implies that  $e_i$  will converge to

$$|e_i| \leq \frac{\bar{s}}{\min_i \{\lambda_{1i}\}} \quad \text{or} \quad |e_i| \leq \left( \frac{\bar{s}}{\min_i \{\lambda_{3i}\}} \right)^{\frac{1}{\gamma}},$$

whereas  $\int_0^t e_i(\tau) d\tau$  will converge to

$$|\int_0^t e_i(\tau) d\tau| \leq \frac{\bar{s}}{\min_i \{\lambda_{2i}\}} \quad \text{or} \quad |\int_0^t e_i(\tau) d\tau| \leq \max_i \left\{ \frac{|e_i(0)|}{\sqrt{\lambda_{2i}}} \right\}.$$

*Case II:*  $|e_i| \leq \varepsilon$ . Substituting (5) into (4) gives

$$\dot{e}_i + \lambda_{1i} e_i + \lambda_{2i} \int_0^t e_i(\tau) d\tau + \lambda_{3i} (\alpha_1 e_i + \alpha_2 \text{sig}(e_i) e_i^2) = s_i. \quad (31)$$

Along analogous steps as Case I, we can rewrite (31) as

$$\begin{aligned} \dot{e}_i + \lambda_{1i} e_i + \left( \lambda_{2i} - \frac{s_i}{\int_0^t e_i(\tau) d\tau} \right) \int_0^t e_i(\tau) d\tau \\ + \lambda_{3i} (\alpha_1 e_i + \alpha_2 \text{sig}(e_i) e_i^2) = 0, \end{aligned}$$

and obtain boundedness of  $e_i$  and  $\int_0^t e_i(\tau) d\tau$ . Proceeding as in Case I and combining the two cases, we obtain convergence of  $e$  in finite-time to the region  $\Phi$  in Theorem 1, and convergence of  $\int_0^t e(\tau) d\tau$  in finite-time to the region  $\bar{\Phi} = \max \{ \max_i \left\{ \frac{|e_i(0)|}{\sqrt{\lambda_{2i}}} \right\}, \frac{\bar{s}}{\min_i \{\lambda_{2i}\}} \} \}$ . The proof is completed.  $\square$

**Remark 2** (Estimation of unstructured uncertainty). *The role of the adaptive law (17) is to estimate the uncertainty (15) without its structural knowledge. In fact, (15) has been derived from EL properties that hold independently of the specific system structure. It is known that nonparametric perturbations may destroy stability of classic adaptive control [34]. As the proposed method achieves stability in the presence of unstructured state-dependent perturbations, it is "robust" in the sense of robust adaptive control.*

**Remark 3** (Modularity). *To illustrate the modular nature of the proposed method, let use (4) and rewrite (16) as:*

$$\mathbf{u}(t) = -\overbrace{\mathbf{\Lambda} \mathbf{s}_1(t)}^{\text{PID action}} - \overbrace{\rho(t) \text{sign}(\mathbf{s}(t)/\mu)}^{\text{Roust-adaptive action}} - \overbrace{-\mathbf{\Lambda} \mathbf{\Lambda}_3 \Delta(\mathbf{e}) - \sigma \text{sig}^\gamma(\mathbf{s}(t))}^{\text{Finite-time action}}, \quad (32)$$

where  $\mathbf{s}_1 = \dot{\mathbf{e}} + \mathbf{\Lambda}_1 \mathbf{e} + \mathbf{\Lambda}_2 \int_0^t \mathbf{e}(\tau) d\tau$ . Similar to the AISMC in [22], (32) allows to augment existing PID loops. The novelty

is to include a finite-time action to better control convergence. The effectiveness of this method will be verified in Sect. IV with comparative experiments with PID and AISMC loops.

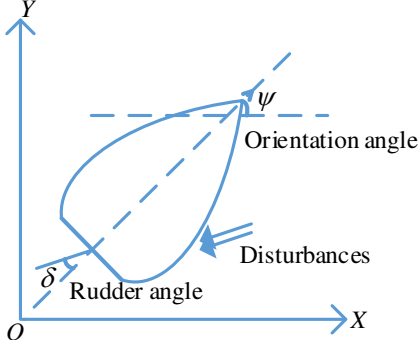


Figure 1: Ship steering scenario.

#### IV. TESTS ON VEHICLES OF DIFFERENT STRUCTURE

We validate the proposed framework into two autopilots: a ship steering autopilot and ArduPlane, the autopilot module of ArduPilot for fixed-wing unmanned aerial vehicles. Let us mention that the ship steering autopilot is quite analogous, in its control architecture, to the steering module of ArduRover in ArduPilot. PID control, a standard ISMC, and the authors' previous AISMC work [22] are used to compare the proposed method. The standard ISMC can be summarized as

$$\mathbf{u}_{\text{ISMC}}(t) = -\Lambda \mathbf{s}_1(t) - \bar{\rho} \text{sign}(\mathbf{s}_1(t)/\mu), \quad (33)$$

while the AISMC can be summarized as

$$\begin{aligned} \mathbf{u}_{\text{AISMC}}(t) &= -\Lambda \mathbf{s}_1(t) - \rho \text{sat}(\mathbf{s}_1(t)/\mu), \\ \rho(t) &= \bar{\theta}_0(t) + \bar{\theta}_1(t) \|\boldsymbol{\xi}(t)\| + \bar{\theta}_2(t) \|\boldsymbol{\xi}(t)\|^2, \\ \dot{\bar{\theta}}_i(t) &= \|\mathbf{s}_1(t)\| \|\boldsymbol{\xi}(t)\|^i - \beta_i \bar{\theta}_i(t), \end{aligned} \quad (34)$$

with  $\mathbf{s}_1(t)$  being the PID term defined after (32) and  $\text{sat}(\cdot/\mu)$ ,  $\mu > 0$  the standard saturation function in  $\pm 1$ . Note that, because the standard ISMC (33) follows a robust (non-adaptive) philosophy, the term  $\bar{\rho}$  is a constant instead of being estimated online. In all the tests we report, we have tuned the gains in (33) to give the best possible performance for PID and ISMC, while we have tuned the gains in the adaptive law (34) to give the best possible performance for AISMC. To make the comparisons as fair as possible,

- the same PID gains  $\Lambda$ ,  $\lambda_1$ ,  $\lambda_2$  are also used in all other methods;
- the same adaptive gains  $\beta_i$  in AISMC are also used in the proposed method.

By doing this, we are able to evaluate if and how much the additional terms in each strategy improve the performance. In AISMC and the proposed method, we use the term  $\text{sat}(\cdot/\mu)$  to replace the corresponding sign function, to allow continuity of the control action that is of practical importance.

##### A. Validation on ship steering autopilot

The motion model of a ship, sketched in Fig. 1, is described via the orientation angle  $\psi$  of the ship controlled by the input rudder angle  $\delta$ , according to the mathematical model [6]

$$T\ddot{\psi} + K \cdot H(\dot{\psi}) = K \cdot \delta + d, \quad (35)$$

where the gain  $K (s^{-1})$  and the time constant  $T (s)$  are function of the ship's constant forward velocity and its length. In (35),  $H(\psi)$  is a nonlinear function: an experiment known as the "spiral test" [35] has shown that  $H(\dot{\psi})$  can be approximated by

$$H(\dot{\psi}) = n_3 \dot{\psi}^3 + n_1 \dot{\psi}, \quad (36)$$

where  $n_1$  and  $n_3$  are real positive constants. The disturbance  $d$  is imposed by the environment. For simulations, the input is also subject to saturation  $\pm 60$  degrees  $\approx \pm 1.05$  radians, and the initial states are set  $[q(0), \dot{q}(0)] = [\psi(0), \dot{\psi}(0)] = [0.4, 0.01]^T$ . To test the tracking capability of the controllers, the desired trajectory is designed to resemble a seesaw [6]: it includes a piecewise constant velocity  $\dot{q}_d = 0.01$  rad/s at  $t \in [0, 15]$ s,  $\dot{q}_d = -0.15$  rad/s at  $t \in [15, 16]$ s, and  $\dot{q}_d = 0.01$  rad/s at  $t \in [16, 30]$ s. To construct all the controllers, we set  $\lambda_1 = 0.83$ ,  $\lambda_2 = 0.02$ ,  $\Lambda = 4.43$ , (PID gains used for all controllers),  $\bar{\rho} = 200$  (used for ISMC),  $\beta_0 = \beta_1 = \beta_2 = 0.01$  with initial values  $\hat{\theta}_0(0) = \hat{\theta}_1(0) = \hat{\theta}_2(0) = 1000$  (used for AISMC and proposed method),  $\lambda_3 = 2.5$ ,  $\epsilon = 3.5$ ,  $\gamma = 0.1$ ,  $\mu = 98$ ,  $\sigma = 30$ , and  $v = 0.7$  (used for proposed method). A combination of the following uncertainty scenarios are considered:

*Uncertain gains* (i.e. not accessible for control design):

- $\mathcal{G}_0$ : constant  $T = 1$ ,  $K = 1$ ,
- $\mathcal{G}_1$ : changing  $T = 1 \rightarrow 0.5$ ,  $K = 1 \rightarrow 2$  at  $t = 10$  s and  $T = 0.5 \rightarrow 2$ ,  $K = 2 \rightarrow 0.5$  at  $t = 20$  s.

*Uncertain disturbance* (i.e. not accessible for control design):

- $\mathcal{D}_0$ :  $d(t) = 0.05 \sin 0.2\pi t$ ,
- $\mathcal{D}_1$ :  $d(t) = 0.1 \sin 0.2\pi t$ .

We obtain four scenarios, reported in Table I, along with the tracking error costs. It is remarkable that the proposed method shows consistent performance in all scenarios with negligible degradation (from 8.71 to 8.72), whereas all the other methods exhibit a much larger performance degradation between the first and the last scenario. Most importantly, since the methods have been designed in such a way to share common gains, Table I validates that

- the robust action of ISMC improves in the range [2-17)% over PID;
- the adaptive action of AISMC improves another [0.3-11)% over ISMC;
- it is the finite-time action of the proposed method that provides the largest improvement, i.e. another [24.5-26.5)% over AISMC.

Table I: Ship steering autopilot: comparisons between tracking error costs for different controllers.

Scenarios	Orientation error $e$ costs			
	Proposed	AISMC	ISMC	PID
$\mathcal{G}_0, \mathcal{D}_0$	<b>8.71</b>	10.84 (+24.5%)	10.87 (+24.8%)	11.06 (+27.0%)
$\mathcal{G}_1, \mathcal{D}_0$	<b>8.71</b>	10.87 (+24.8%)	11.10 (+27.4 %)	11.59 (+33.1%)
$\mathcal{G}_0, \mathcal{D}_1$	<b>8.72</b>	10.89 (+24.9%)	11.10 (+27.3%)	11.47 (+31.5%)
$\mathcal{G}_1, \mathcal{D}_1$	<b>8.72</b>	11.03 (+26.5%)	12.03 (+38.0%)	13.54 (+55.3%)

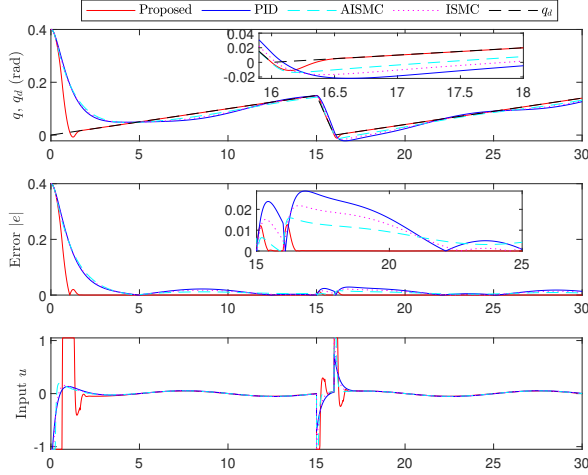


Figure 2: Ship steering: tracking performance for the orientation angle  $\psi$  ( $q$ ), norm of the tracking error and control input, with uncertainty scenario  $\mathcal{G}_0, \mathcal{D}_0$  (cf. Table I).

This validate the effectiveness of the proposed method in delivering the largest improvement. For compactness, the tracking performance, tracking error and control input are reported in Figs. 2-3 only for the first and the last scenario of Table I. The figures and the table show that the proposed method has faster convergence to the target angle (let us remark that this faster convergence is only obtained via the finite-time action, since all controllers share the same PID gains): although this faster convergence is clearly achieved via larger and more reactive input, it is remarkable that the proposed method can deal with input saturation despite this was treated *on purpose* as unmodelled dynamics (i.e. treated as an extra source of uncertainty).

### B. Validation on ArduPilot autopilot

The validations adopt a software-in-the-loop (SITL) environment, meaning that we test the actual open-source ArduPilot suite [36]. Fig. 4 illustrates the SITL architecture. For control, ArduPilot relies on a philosophy that aims to approximate the vehicle dynamics with second-order dynamics, and close them with PID loops [36]. Such a philosophy is supported by standard literature like [37], which we explain as follows.

It is well known that the 6-DOF fixed-wing dynamics are coupled and complex [37, Chapt. 3]. So, several literature suggests to simplify the control design via low-order models (refer to [37, Chapt. 5] for a details). For compactness, let us use the transfer function notation to describe the relation

Table II: Parameter selection for the proposed method

Loop	$\gamma$	$\varepsilon$	$\lambda_3$	$\beta_i$ $i=0,1,2$	$\mu$	$v$	$\sigma$
pitch	$10^{-3}$	10	$10^{-3}$	10	420	0.8	3.6
roll	$10^{-3}$	10	$10^{-3}$	160	1000	0.95	0.001
yaw	$10^{-3}$	10	$10^{-3}$	0.001	0.001	0.5	1.4
TECS throttle	$10^{-3}$	10	$10^{-3}$	0.001	10.4	0.01	0.04
TECS pitch	$10^{-3}$	10	$10^{-3}$	4	44	0.47	0.05

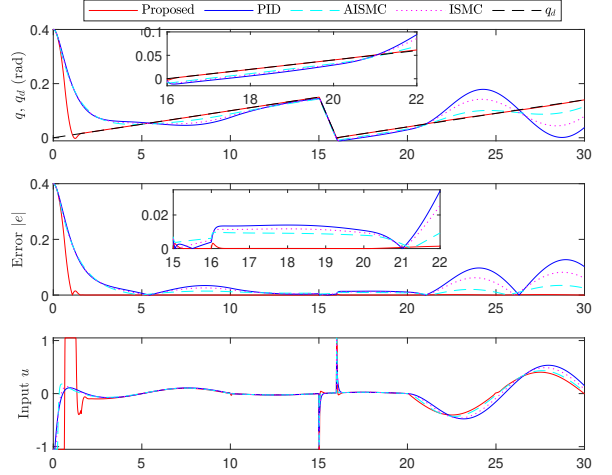


Figure 3: Ship steering: tracking performance for the orientation angle  $\psi$  ( $q$ ), norm of the tracking error and control input, with uncertainty scenario  $\mathcal{G}_1, \mathcal{D}_1$  (cf. Table I).

between the elevator deflection  $\delta_e$  and the pitch angle  $\theta$ , between the pitch angle  $\theta$  and the altitude  $h$ , and between the throttle  $\delta_t$  and pitch angle  $\theta$  to the airspeed  $V_a$ . These are the main components of the longitudinal dynamics:

$$\begin{aligned} \text{pitch} \quad \theta(s) &= \frac{a_{\theta 3}}{s^2 + a_{\theta 1}s + a_{\theta 2}} (\delta_e(s) + \frac{1}{a_{\theta 3}} d_{\theta 2}(s)), \\ \text{altitude} \quad h(s) &= \frac{V_a}{s} (\theta(s) + \frac{1}{V_a} d_h(s)), \\ \text{airspeed} \quad \bar{V}_a(s) &= \frac{1}{s + a_{v_1}} (a_{v_2} \bar{\delta}_t(s) - a_{v_3} \bar{\theta}(s) + d_v(s)), \end{aligned} \quad (37)$$

where  $a_{\theta 1} \triangleq -\frac{\rho_a V_a^2 c S}{2 J_y} C_{m_q} \frac{c}{2 V_a}$ ,

$$\begin{aligned} a_{\theta 2} &\triangleq -\frac{\rho_a V_a^2 c S}{2 J_y} C_{m_\alpha}, \quad a_{\theta 3} \triangleq \frac{\rho_a V_a^2 c S}{2 J_y} C_{m_{\delta_e}}, \\ d_{\theta 2} &\triangleq \Gamma_6(r^2 - p^2) + \Gamma_5 pr + \frac{\rho_a V_a^2 c S}{2 J_y} [C_{m_0} - C_{m_\alpha} \gamma - C_{m_q} \frac{c}{2 V_a} d_{\theta 1}] + \dot{d}_{\theta 1}, \\ d_h &\triangleq (u \sin \theta - V_a \theta) - v \sin \phi \cos \theta - w \cos \phi \cos \theta, \\ \bar{V}_a &\triangleq V_a - V_a^* \text{ is the deviation of } V_a \text{ from trim } V_a^*, \\ \bar{\theta} &\triangleq \theta - \theta^* \text{ is the deviation of } \theta \text{ from trim } \theta^*, \\ \bar{\delta}_t &\triangleq \delta_t - \delta_t^* \text{ is the deviation of } \delta_t \text{ from trim } \delta_t^*, \\ a_{v_1} &\triangleq \frac{\rho V_a^* S}{m_u} (C_{D_0} + C_{D_{\alpha^*}} + C_{D_{\delta_e}} \delta_e^*) + \frac{\rho S_{\text{prop}}}{m_u} C_{\text{prop}} V_a^*, \\ a_{v_2} &\triangleq \frac{\rho S_{\text{prop}}}{m_u} C_{\text{prop}} k_{\text{motor}}^2 \delta_t^*, \quad a_{v_3} \triangleq g \cos(\theta^* - \chi^*), \end{aligned}$$

where  $\phi$  is the Euler roll angle,  $p, r$  are the roll rate and yaw rate in body frame,  $\gamma$  is flight path angle,  $\chi^*$  is the course angle trim and the terms  $C_{m_q}, C_{m_\alpha}, C_{m_{\delta_e}}, C_{m_0}, C_{D_0}, C_{D_{\alpha^*}}, C_{D_{\delta_e}}$  are Taylor approximations of aerodynamic coefficients. We do not report the lateral dynamics for compactness, the interested reader is referred to [37, Chapt. 5]. It is worth remarking that most coefficients in (37) are uncertain and difficult to identify, as they might change with time and with the operating

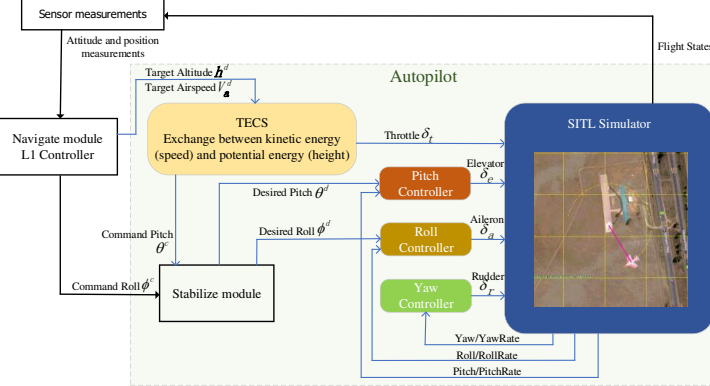


Figure 4: SITL architecture in ArduPilot: the Navigate module (L1 controller) sends guidance commands to the TECS and the Stabilize modules; from there, roll-pitch-yaw attitude controllers act on the corresponding servo motors.

conditions. Additionally,  $d_{\theta 2}$ ,  $d_h$ ,  $d_v$  represent complex state-dependent disturbances coming from the coupled dynamics. These issues make model-based or structure-based autopilots hard to implement in practice: meanwhile, non-adaptive PID loops may guarantee practical stability, but whether such a loops are effective in the presence of state-dependent uncertainty is questionable, as shown later in our tests.

Since ArduPilot relies on closing the vehicle dynamics with PID loops [36], by recalling (32), we have the opportunity to test the proposed method by augmenting the original loops of ArduPilot. Indeed, the attitude control modules in Fig. 4 can either contain the original ArduPilot autopilot, or a user-designed autopilot (e.g., the AISMC [22] or the approach proposed in this work). As the original ArduPilot consists of a family of PID loops, one can choose  $\Lambda, \lambda_1, \lambda_2$  in (16) as the PID gains set in the ArduPilot code [36]. The other parameters for the proposed approach are listed in Table II.

To evaluate the robustness of the proposed autopilot under large uncertainty, the mass of the UAV will be changed during the flight (which can represent some change in the payload). The initial mass is 2kg, and it can change to half mass (1kg) or

Table III: Tracking error costs for proposed, original PID and AISMC autopilots. The percentage degradation with respect to the proposed method is indicated.

Mass	Proposed autopilot					
	Roll	Pitch	Yaw	TECS throttle	TECS pitch	Total
2 → 1kg	1.34	0.99	5.31	2.75	2.55	<b>12.94</b>
2kg	1.01	1.01	0.49	0.51	0.65	<b>3.67</b>
2 → 4kg	0.8	1.07	3.52	1.73	2.55	<b>9.67</b>
Mass	Original PID autopilot					
	Roll	Pitch	Yaw	TECS throttle	TECS pitch	Total
2 → 1kg	1.38	0.88	5.68	10.33	3.09	21.36 (+65.1%)
2kg	1	1	1	1	1	5.0 (+36.2%)
2 → 4kg	0.72	1.3	4.0	5.43	5.9	17.35 (+79.4%)
Mass	AISMC autopilot					
	Roll	Pitch	Yaw	TECS throttle	TECS pitch	Total
2 → 1kg	1.47	0.94	5.44	4.94	2.97	15.76 (+21.8%)
2kg	1	1	0.49	0.73	0.92	4.14 (+12.8%)
2 → 4kg	0.78	1.17	3.6	2.55	3.9	12.0 (+24.1%)

double mass (4kg) during flight. Neither the mass nor the mass change is known a priori, which allows to test how different autopilots cope with this uncertainty. The flight includes a take-off phase, a cruising phase (orbiting constant altitude and constant airspeed), and a landing phase. Note that the mass change occurs during the cruising phase. Table III reports the tracking error costs for the different autopilots under different mass conditions. Five control loops are reported, representing the main loops of a fixed-wing UAV: roll, pitch, yaw, TECS throttle and TECS pitch. The term TECS means total energy control system, i.e. the control loops for altitude (potential energy) and speed (kinetic energy). The cost accounts for the tracking errors with respect to the desired roll, pitch, yaw, potential and kinetic energy. The performance of the original PID autopilot with constant 2kg mass is used as a normalizing factor, so that the cost is 5.0 in this scenario. The table shows that the tracking error costs of the proposed autopilot are smaller than other autopilots under both constant mass scenario and changing mass scenario: the proposed autopilot overcomes the original autopilot by more than 36.2% for the original PID autopilot and by more than 12.8% for the AISMC autopilot. The enhanced performance is especially evident in the changing mass scenario.

To visualize the performance in the changing mass scenario, relevant flight variables are visualized in Figs. 5 and 6 for the proposed, the original PID and the AISMC autopilots. As shown in Figs. 5a and 6a, the proposed autopilot has negligible altitude drop after mass change. Figs. 5b and 6b show the faster reaction in pitch demand, with reasonable elevator input. Figs. 5c and 6c show that the airspeed of the proposed autopilot has smaller overshoot and converges faster. As shown in Figs. 5d and 6d, the throttle for the proposed solution is more reactive in response to the mass change.

To conclude, the tests show that the proposed method overcomes the other ones in terms of robustness and adaptation, suggesting more effectiveness in tackling state-dependent uncertainty typically arising in autopilot applications.

## V. CONCLUSIONS AND FUTURE WORK

This paper explored a novel boundary-layer Euler-Lagrange (EL) control method not relying on structural knowledge of the system dynamics. Design considerations and software-in-the-loop tests have shown the capability of the proposed solution to be integrated in existing autopilot loops, with enhanced robustness and adaptation performance. Future work will aim to test several modules in open-source autopilots meant for vehicles with different structure (copters, vessels, rovers, etc.). A preliminary study in this sense is [38]. A problem in the field of unstructured uncertainties is to consider unmatched/unactuated terms: this could deserve further research. Also, as structure-free EL methods exist based on prescribed performance or funnel functions [39], [40], it is of interest to explore similarities and differences with the proposed method, or their implementation in autopilot architectures.

## REFERENCES

- [1] F. Santoso, M. A. Garratt, and S. G. Anavatti, "Hybrid PD-fuzzy and PD controllers for trajectory tracking of a quadrotor unmanned aerial

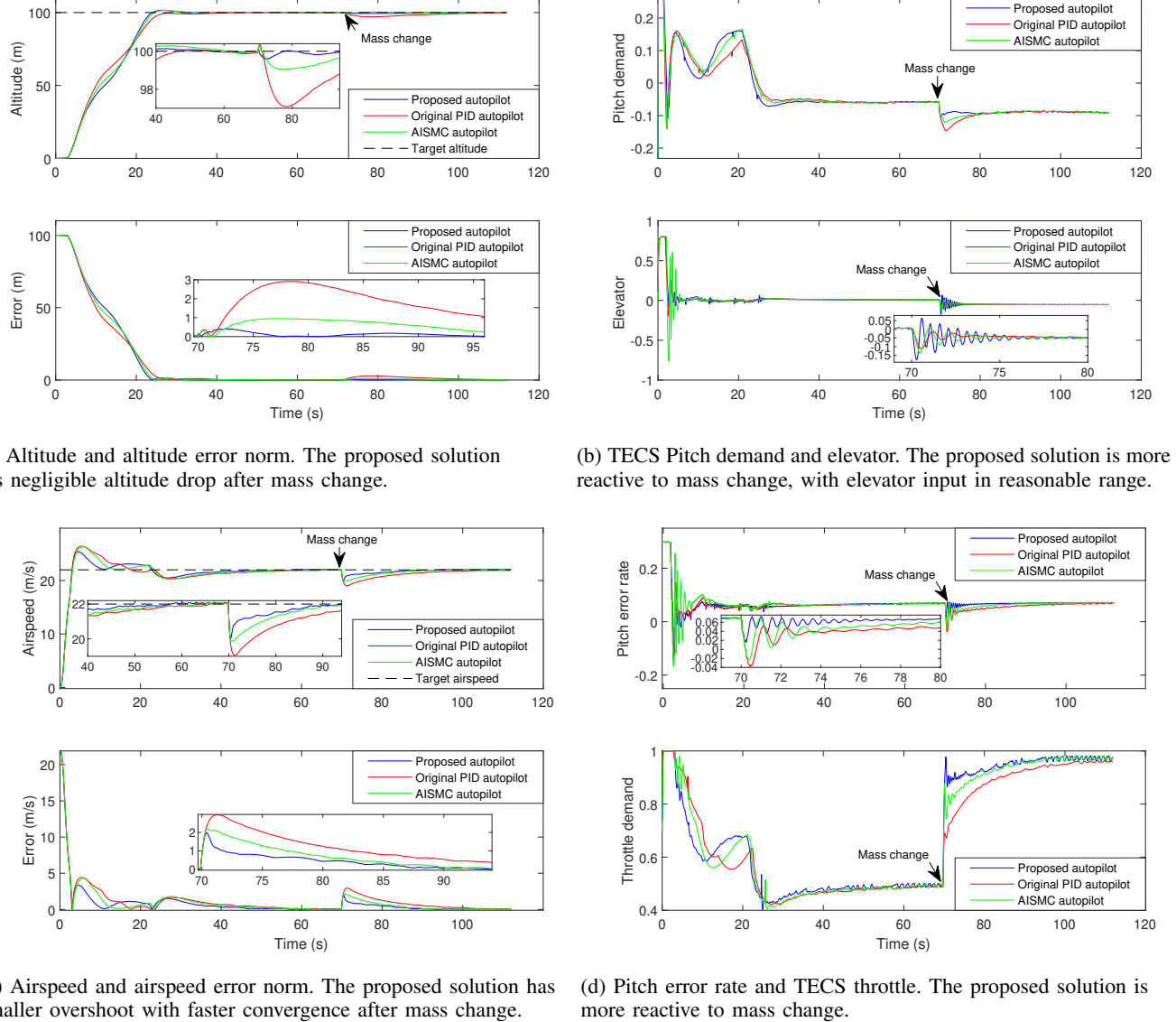


Figure 5: Mass change  $2.0\text{kg} \rightarrow 1.0\text{kg}$ : comparison of proposed, original PID and AISMC [22] autopilots.

- vehicle: Autopilot designs and real-time flight tests,” *IEEE Transactions on Systems, Man, and Cybernetics: Systems*, vol. 51, no. 3, pp. 1817–1829, 2021.
- [2] S. Baldi, S. Roy, K. Yang, and D. Liu, “An underactuated control system design for adaptive autopilot of fixed-wing drones,” *IEEE/ASME Transactions on Mechatronics*, pp. 1–12, 2022.
  - [3] P. Li, D. Liu, and S. Baldi, “Plug-and-play adaptation in autopilot architectures for unmanned aerial vehicles,” in *IECON 2021 – 47th Annual Conference of the IEEE Industrial Electronics Society*, 2021, pp. 1–6.
  - [4] H. Dong and J. Xi, “Model predictive longitudinal motion control for the unmanned ground vehicle with a trajectory tracking model,” *IEEE Transactions on Vehicular Technology*, vol. 71, no. 2, pp. 1397–1410, 2022.
  - [5] K. D. von Ellenrieder, S. C. Licht, R. Belotti, and H. C. Henninger, “Shared human–robot path following control of an unmanned ground vehicle,” *Mechatronics*, vol. 83, p. 102750, 2022.
  - [6] G. Rigatos and S. Tzafestas, “Adaptive fuzzy control for the ship steering problem,” *Mechatronics*, vol. 16, no. 8, pp. 479–489, 2006.
  - [7] B. Kürkçü and C. Kasnakoğlu, “Robust autopilot design based on a disturbance/uncertainty/coupling estimator,” *IEEE Transactions on Control Systems Technology*, vol. 27, no. 6, pp. 2622–2629, 2019.
  - [8] C. Fu, A. Sarabakha, E. Kayacan, C. Wagner, R. John, and J. M. Garibaldi, “Input uncertainty sensitivity enhanced nonsingleton fuzzy logic controllers for long-term navigation of quadrotor UAVs,” *IEEE/ASME Transactions on Mechatronics*, vol. 23, no. 2, pp. 725–734, 2018.
  - [9] Z. Yang, J. Huang, H. Yin, D. Yang, and Z. Zhong, “Path tracking control for underactuated vehicles with matched-mismatched uncertainties: An uncertainty decomposition based constraint-following approach,” *IEEE Transactions on Intelligent Transportation Systems*, pp. 1–14, 2021.
  - [10] S. Roy, S. Baldi, P. Li, and V. Narayanan, “Artificial-delay adaptive control for under-actuated Euler–Lagrange robotics,” *IEEE/ASME Transactions on Mechatronics*, pp. 1–1, 2021.
  - [11] M. G. Safonov, “Robust control: Fooled by assumptions,” *International Journal of Robust and Nonlinear Control*, vol. 28, no. 12, pp. 3667–3677, 2018.
  - [12] M. M. Rayguru, R. E. Mohan, R. Parween, L. Yi, A. V. Le, and S. Roy, “An output feedback based robust saturated controller design for pavement sweeping self-reconfigurable robot,” *IEEE/ASME Transactions on Mechatronics*, vol. 26, no. 3, pp. 1236–1247, 2021.
  - [13] E. Nuño and R. Ortega, “Achieving consensus of Euler–Lagrange agents with interconnecting delays and without velocity measurements via passivity-based control,” *IEEE Transactions on Control Systems Technology*, vol. 26, no. 1, pp. 222–232, 2018.
  - [14] L. Yu, G. He, X. Wang, and S. Zhao, “Robust fixed-time sliding

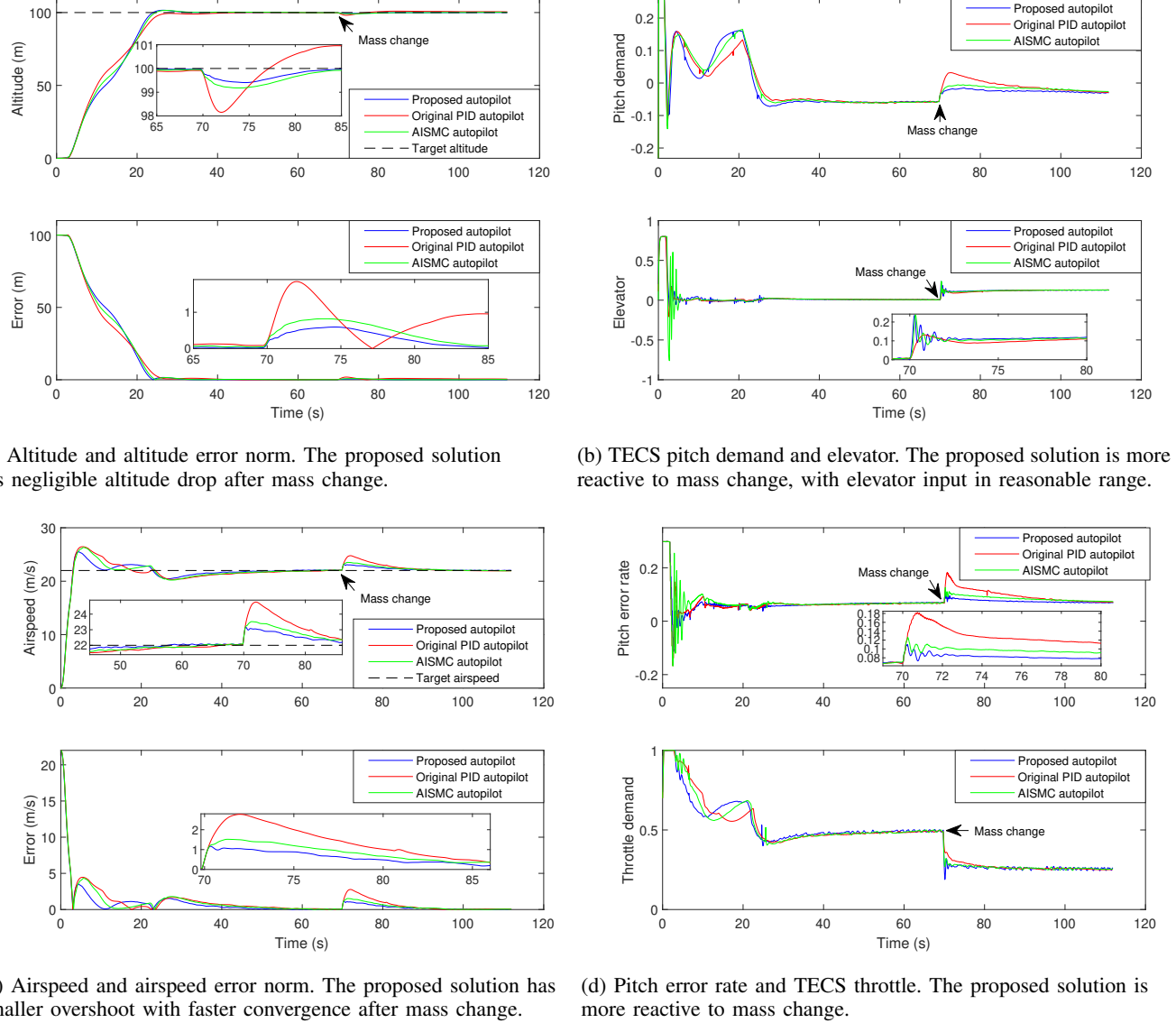


Figure 6: Mass change  $2.0\text{kg} \rightarrow 4.0\text{kg}$ : comparison of proposed, original PID and AISMC [22] autopilots.

mode attitude control of tilt tri-rotor UAV in helicopter mode,” *IEEE Transactions on Industrial Electronics*, pp. 1–1, 2021.

- [15] L. Wan, Y.-J. Pan, and H. Shen, “Improving synchronization performance of multiple Euler-Lagrange systems using non-singular terminal sliding mode control with fuzzy logic,” *IEEE/ASME Transactions on Mechatronics*, pp. 1–1, 2021.
- [16] C. Ma, J. Lam, and F. L. Lewis, “Trajectory regulating model reference adaptive controller for robotic systems,” *IEEE Transactions on Control Systems Technology*, vol. 27, no. 6, pp. 2749–2756, 2019.
- [17] T. Souanef, “ $\mathcal{L}_1$  adaptive path-following of small fixed-wing unmanned aerial vehicles in wind,” *IEEE Transactions on Aerospace and Electronic Systems*, pp. 1–1, 2022.
- [18] K. Shao, J. Zheng, R. Tang, X. Li, Z. Man, and B. Liang, “Barrier function based adaptive sliding mode control for uncertain systems with input saturation,” *IEEE/ASME Transactions on Mechatronics*, vol. 27, no. 6, pp. 4258–4268, 2022.
- [19] F. Plestan, Y. Shtessel, V. Brégeault, and A. Poznyak, “New methodologies for adaptive sliding mode control,” *International Journal of Control*, vol. 83, no. 9, pp. 1907–1919, 2010.
- [20] C. Edwards and Y. B. Shtessel, “Adaptive continuous higher order sliding mode control,” *Automatica*, vol. 65, pp. 183–190, 2016.
- [21] Y. Hu, H. Wang, S. He, J. Zheng, and Z. Man, “Adaptive tracking control of an electronic throttle valve based on recursive terminal sliding mode,”

*IEEE Transactions on Vehicular Technology*, vol. 1, no. 1, pp. 1–11, 2020.

- [22] P. Li, D. Liu, and S. Baldi, “Adaptive integral sliding mode control in the presence of state-dependent uncertainty,” *IEEE/ASME Transactions on Mechatronics*, pp. 1–11, 2022.
- [23] S. Roy, J. Lee, and S. Baldi, “A new adaptive-robust design for time delay control under state-dependent stability condition,” *IEEE Transactions on Control Systems Technology*, vol. 29, no. 1, pp. 420–427, 2021.
- [24] C. D. Cruz-Ancona, M. A. Estrada, and L. Fridman, “Barrier function-based adaptive lyapunov redesign for systems without a priori bounded perturbations,” *IEEE Transactions on Automatic Control*, vol. 67, no. 8, pp. 3851–3862, 2022.
- [25] H. Haimovich, L. Fridman, and J. A. Moreno, “Generalized super-twisting for control under time- and state-dependent perturbations: Breaking the algebraic loop,” *IEEE Transactions on Automatic Control*, vol. 67, no. 10, pp. 5646–5652, 2022.
- [26] S. Roy, S. Baldi, and L. M. Fridman, “On adaptive sliding mode control without a priori bounded uncertainty,” *Automatica*, vol. 111, p. 108650, 2020.
- [27] N. Wang, C. Qian, J.-C. Sun, and Y.-C. Liu, “Adaptive robust finite-time trajectory tracking control of fully actuated marine surface vehicles,” *IEEE Transactions on Control Systems Technology*, vol. 24, no. 4, pp.

- 1454–1462, 2016.
- [28] O. Mofid and S. Mobayen, “Adaptive finite-time back-stepping global sliding mode tracker of quad-rotor UAVs under model uncertainty, wind perturbation and input saturation,” *IEEE Transactions on Aerospace and Electronic Systems*, pp. 1–1, 2021.
- [29] X. Yu, Y. Feng, and Z. Man, “Terminal sliding mode control – an overview,” *IEEE Open Journal of the Industrial Electronics Society*, vol. 2, pp. 36–52, 2021.
- [30] G. P. Incremona, M. Cucuzzella, and A. Ferrara, “Adaptive suboptimal second-order sliding mode control for microgrids,” *International Journal of Control*, vol. 89, no. 9, pp. 1849–1867, 2016.
- [31] F. Wang, B. Chen, C. Lin, J. Zhang, and X. Meng, “Adaptive neural network finite-time output feedback control of quantized nonlinear systems,” *IEEE Transactions on Cybernetics*, vol. 48, no. 6, pp. 1839–1848, 2018.
- [32] H. Yang and D. Ye, “Adaptive fixed-time bipartite tracking consensus control for unknown nonlinear multi-agent systems: An information classification mechanism,” *Information Sciences*, pp. 238–254, 2018.
- [33] Z. Zuo, “Nonsingular fixed-time consensus tracking for second-order multi-agent networks,” *Automatica*, vol. 54, pp. 305–309, 2015.
- [34] P. Ioannou and J. Sun, *Robust Adaptive Control*. Dover Publications, 2012.
- [35] J. Layne and K. Passino, “Fuzzy model reference learning control for cargo ship steering,” *IEEE Control Systems Magazine*, vol. 13, no. 6, pp. 23–34, 1993.
- [36] “Open source for ardupilot open source autopilot,” Online, <https://github.com/ArduPilot/ardupilot>.
- [37] R. W. Beard and T. W. McLain, *Small Unmanned Aircraft Theory and Practice*. Princeton University Press, 2012.
- [38] P. Li, D. Liu, X. Xia, and S. Baldi, “Embedding adaptive features in the ardupilot control architecture for unmanned aerial vehicles,” in 2022 *IEEE 61st Conference on Decision and Control (CDC)*, 2022, pp. 3773–3780.
- [39] C. K. Verginis and D. V. Dimarogonas, “Asymptotic stability of uncertain lagrangian systems with prescribed transient response,” in 2019 *IEEE 58th Conference on Decision and Control (CDC)*, 2019, pp. 7037–7042.
- [40] ——, “Asymptotic tracking of second-order nonsmooth feedback stabilizable unknown systems with prescribed transient response,” *IEEE Transactions on Automatic Control*, vol. 66, no. 7, pp. 3296–3302, 2021.



**Peng Li** received the B.Sc. in electronic information from Hubei University of Science and Technology, China, in 2013, and the M.Tech. in electronic science and technology from Wuhan University of Technology, China, in 2016. After that, he worked as a software engineer and he is currently pursuing the PhD in cyber science and engineering at Southeast University, China. His research interests includes adaptive nonlinear control and its applications to unmanned vehicles.



**Di Liu** (M’22) received the B.Sc. in information science from Hubei University of Science and Technology, and the M.Sc. in control science and engineering from Chongqing University of Posts and Telecommunications in 2014 and 2017. She received a first Ph.D. in cyber science and engineering from Southeast University, China, in 2021 and a second Ph.D. in systems and control from University of Groningen, The Netherlands, in 2022. She is now pursuing postdoctoral studies with School of Computation, Information and Technology, Technische

Universitat Munchen (TUM), Germany. Her research interests are learning systems and control, with application in intelligent transportation, automated vehicles, unmanned aerial vehicles.



**Simone Baldi** (M’14-SM’19) received the B.Sc. in electrical engineering, and the M.Sc. and Ph.D. in automatic control engineering from University of Florence, Italy, in 2005, 2007, and 2011, respectively. He is professor at Southeast University, with a guest position at Delft Center for Systems and Control, TU Delft, where he was assistant professor. He was awarded outstanding reviewer of *Applied Energy* (2016) and *Automatica* (2017). He is subject editor of *International Journal of Adaptive Control and Signal Processing*, technical editor of *IEEE/ASME Transactions on Mechatronics*, associate editor of *IEEE Control Systems Letters* and *Journal of the Franklin Institute*. His research interests include adaptive and learning systems with applications in networked control, unmanned systems, and intelligent vehicles.